

AD-A072 987

AIR FORCE GEOPHYSICS LAB HANSCOM AFB MA

F/G 4/1

A DYNAMICAL MODEL FOR THE ONSET OF MAGNETOSPHERIC SUBSTORMS.(U)

DEC 78 P L ROTHWELL, G K YATES

AFGL-TR-78-0306

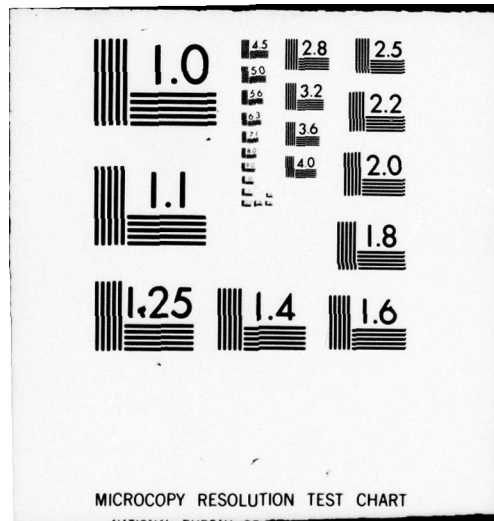
NL

UNCLASSIFIED

| OF |

AD4  
072987





DA072987

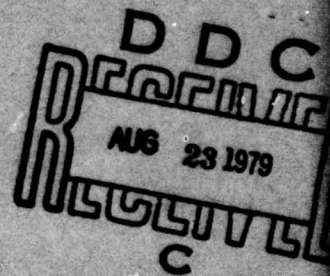
AFGL-TR-78-0306  
ENVIRONMENTAL RESEARCH PAPERS, NO. 847

LEVEL IV



## A Dynamical Model for the Onset of Magnetospheric Substorms

P. L. ROTHWELL  
G. K. YATES



13 December 1978

Approved for public release; distribution unlimited.

DDC FILE COPY

SPACE PHYSICS DIVISION    PROJECT 7601  
AIR FORCE GEOPHYSICS LABORATORY  
HANSCOM AFB, MASSACHUSETTS 01731

AIR FORCE SYSTEMS COMMAND, USAF



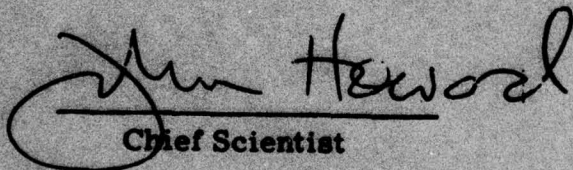
79 08 22 001



This report has been reviewed by the ESD Information Office (OI) and is releasable to the National Technical Information Service (NTIS).

This technical report has been reviewed and is approved for publication.

FOR THE COMMANDER

  
Chief Scientist

Qualified requestors may obtain additional copies from the Defense Documentation Center. All others should apply to the National Technical Information Service.



Unclassified

SECURITY CLASSIFICATION OF THIS PAGE (When Data Entered)

REPORT DOCUMENTATION PAGE		READ INSTRUCTIONS BEFORE COMPLETING FORM	
1. REPORT NUMBER	2. GOVT ACCESSION NO.	3. RECIPIENT'S CATALOG NUMBER	
(14) AFGL-TR-78-0306	AFGL-ERP-647		
4. TITLE (and Subtitle)		5. TYPE OF REPORT & PERIOD COVERED	
(6) A DYNAMICAL MODEL FOR THE ONSET OF MAGNETOSPHERIC SUBSTORMS		Scientific. Interim.	
7. AUTHOR(s)		6. PERFORMING ORG. REPORT NUMBER	
(10) P. L. Rothwell G. K. Yates		ERP No. 647	
8. CONTRACT OR GRANT NUMBER(s)			
9. PERFORMING ORGANIZATION NAME AND ADDRESS		10. PROGRAM ELEMENT, PROJECT, TASK AREA & WORK UNIT NUMBERS	
Air Force Geophysics Laboratory (PHG) Hanscom AFB Massachusetts 01731		(16) 76011202 (17) 12	
11. CONTROLLING OFFICE NAME AND ADDRESS		12. REPORT DATE	
Air Force Geophysics Laboratory (PHG) Hanscom AFB Massachusetts 01731		(11) 13 December 1978	
13. MONITORING AGENCY NAME & ADDRESS (if different from Controlling Office)		14. NUMBER OF PAGES	
(12) 44 p.		46	
15. SECURITY CLASS. (of this report)		15a. DECLASSIFICATION/DOWNGRADING SCHEDULE	
Unclassified			
16. DISTRIBUTION STATEMENT (of this Report)			
Approved for public release; distribution unlimited.			
17. DISTRIBUTION STATEMENT (of the abstract entered in Block 20, if different from Report)			
(9) Environmental research papers,			
18. SUPPLEMENTARY NOTES			
19. KEY WORDS (Continue on reverse side if necessary and identify by block number)			
Substorm Magnetic instabilities Field-line reconnection Multiple onsets			
20. ABSTRACT (Continue on reverse side if necessary and identify by block number)			
A model for the onset of magnetospheric substorms is developed based on the observations of Pytte et al (1976). North-south single-particle motion across the plasma sheet becomes instrumental in generating magnetic instabilities when the plasma sheet is sufficiently compressed. The number density times the square of the plasma sheet thickness is found to be the critical parameter ( $n l^2 \leq 8.1 \times 10^{15}$ protons/cm). A merging theory is developed based on these magnetic instabilities. The nightside merging rate is controlled by			

CONT →

DD FORM 1 JAN 73 1473

EDITION OF 1 NOV 65 IS OBSOLETE

Unclassified

SECURITY CLASSIFICATION OF THIS PAGE (When Data Entered)

( $n l^2$  squared less than or equal to  $8.1 \times 10^{15}$  to the 15th power

409 578

✓

Unclassified

SECURITY CLASSIFICATION OF THIS PAGE (When Data Entered)

20. Abstract (Continued)

CONT → the value of the magnetic field in the tail lobes which, in turn, is dependent on the dayside merging rate. Merging and collisional damping of the  $J \times B$  force contribute to the heating of the plasma sheet. The 10-15 min interval between onsets is interpreted in terms of a weak coupling between the tail lobes and the plasma sheet. A straightforward application of small-amplitude oscillation theory shows that the period between onsets is a direct measure of the mean collision frequency in the plasma sheet. The obtained value is in good agreement with that calculated from the resistivity relation.

Unclassified

SECURITY CLASSIFICATION OF THIS PAGE (When Data Entered)



## Preface

We would like to express our appreciation to Dr. John F. McClay for many helpful discussions and to Drs. Henry B. Garrett, David A. Hardy and William Burke for their comments and reading of the manuscript. Particular thanks is extended to Professors R. Wolf and P. Rieff of Rice University for their help and encouragement.

Accession For		<input checked="checked" type="checkbox"/> <input type="checkbox"/> <input type="checkbox"/>
NTIS GRI&I		
DDC TAB		
Unannounced Justification		
By _____		
Distribution/ _____		
Availability Codes		
Dist	Avail and/or special	
A		



## Contents

1. INTRODUCTION	7
2. THE PLASMA SHEET	9
3. MERGING	16
4. MAGNETOTAIL OSCILLATIONS	23
5. SUMMARY AND CONCLUSIONS	29
REFERENCES	31
BIBLIOGRAPHY	33
APPENDIX A: Single Particle Trajectories	35
APPENDIX B: Solution of the Eigenmodes	43

## Illustrations

1. A Schematic Representation of the Earth's Magnetotail	17
2. Assumption: There Exists a Power Density Spectrum for Magnetic Fluctuations as a Function $f'_m$	20
3. The Magnetotail Modeled as Three Coupled Oscillators	25
4. The Four Possible Eigenmodes of the Coupled Oscillator System Shown in Figure 3	26

## Illustrations

A1. Various Proton Trajectories that Illustrate the Several Regimes of $V_y$ as Shown in Figure A2	38
A2. Proton Drift Velocity in the Plasma Sheet as a Function of Energy	40
B1. Energy Matrix for the Configuration Shown in Figure 3	46

## A Dynamical Model for the Onset of Magnetospheric Substorms

### 1. INTRODUCTION

The purpose of this paper is to develop a dynamical model for the onset of magnetospheric substorms based on experimental observations by Pytte et al.<sup>1</sup> We require this model to contain: (1) a "triggering" mechanism that is related to the compression of the plasma sheet; (2) a merging process which is governed by magnetic (current) fluctuations; and (3) a mechanism that explains multiple onsets.

Present steady-state merging theories fall into two general categories: (1) self-consistency conditions between the convected particles and the crosstail current (Alfven,<sup>2</sup> and Dessler<sup>3</sup>), and (2) dissipation models for the conversion of magnetic energy into joule heating (Sweet,<sup>4</sup> Parker,<sup>5</sup> and Coppi and Friedland<sup>6</sup>). An excellent review article by Vasyliunas<sup>7</sup> also treats the standing shock theory of Petschek.<sup>8</sup>

Approach: The behavior of the plasma sheet is governed by the relative values of the mean collision time, the proton gyro-period and the characteristic transit time of the  $\mathbf{J} \times \mathbf{B}$  force. The latter will be explained in detail later. We first assume and then show, that if the mean proton collision time is sufficiently long

---

(Received for publication 11 December 1978)

Due to the number of references to be included as footnotes on this page, the reader is referred to the list of references, page 31.



that a finite number of protons can travel across the plasma sheet without being diverted by collisions. These protons are simply responding to the  $\mathbf{J} \times \mathbf{B}$  force.

With the magnetic field measurements of Bowling and Wolf,<sup>9</sup> the  $\mathbf{J} \times \mathbf{B}$  equation of force turns out to be that of a harmonic oscillator. It is shown that in order for the harmonic component to be significant that  $n l^2 < 8.1 \times 10^{15}$  protons/cm. For  $n \approx 0.3$  protons/cm<sup>3</sup>, this condition is satisfied if the north-south thickness of the plasma sheet,  $l$ , is less than 1634 km. Thus compression of the plasma sheet by the tail lobes enhances the harmonic component. This in turn is identified as a time-dependent "triggering" mechanism. An individual particle treatment given in Appendix A leads to a similar conclusion.

In Section 3, the effects of a localized interruption of the cross-tail current are analyzed. If the interruption occurs near the neutral sheet, then symmetric magnetic field line deformations will occur at the plasma sheet-tail lobe interfaces. If the harmonic oscillator triggering mechanism is present, the deformed magnetic field lines may merge. It is found that one of the necessary conditions for the process is related to and thus controlled by the daytime merging rate.

In Section 4, we develop a simple dynamical model for multiple onsets. Force constants for the tail lobes are derived by treating transverse compressional waves as being equivalent to a density of harmonic oscillators. These force constants, coupled to that of the simple harmonic component in the plasma sheet (Section 2), represent a three-oscillator system. The eigenmodes of this system are derived in the standard fashion. One of the four possible eigenmodes corresponds to a displacement of both tail lobes towards the neutral sheet. It is this mode one expects to be excited during magnetic substorms. The corresponding eigenperiod is a sensitive measure of the simple harmonic oscillator component in the plasma sheet (Section 2) and of the mean proton collision frequency.

The physical picture of a substorm according to this model is as follows: Simultaneous displacement of both tail lobes towards the neutral sheet compresses the plasma sheet. When this compression is sufficiently intense, a harmonic component can then be maintained across the neutral sheet. This component allows sporadic merging to occur where the merging rate is controlled by the magnetic noise power density spectrum and the value of  $B$  in the tail lobes. Upon expansion of the plasma sheet, the harmonic component cannot be maintained and merging stops. This process is repeated periodically until enhanced turbulence damps all coherent (oscillatory) motion.

**B-Field Data:** The two-component steady-state and time-dependent model is supported by magnetic field data taken in the plasma sheet from Explorer 34

9. Bowling, S.B., and Wolf, R. A. (1974) The motion and magnetic structure of the plasma sheet near 30  $R_E$ , Planet. Space Sci. 22:673.

(Bowling and Wolf<sup>9</sup>). Bowling and Wolf<sup>9</sup> showed that the average x-component of the tail magnetic field varied linearly on either side of the neutral sheet. In contrast, Garrett<sup>10</sup> showed the significant presence of ULF magnetic fluctuations over short time-scales using the same data. In this paper we take the point of view that the averaged, linear B-field acts on the protons mentioned above. This leads to the harmonic particle component. The ULF fluctuations are considered to be caused either by the sporadic merging as described in Section 3 or by the oscillation modes described in Section 4.

Definitions: The plasma sheet is taken to be the region in the earth's geomagnetic tail that lies above and below the neutral sheet and is characterized by a magnetic depression (Garrett<sup>10</sup>). The neutral sheet is defined to be the  $z = 0$  plane where  $B_x$  reverses sign. For purposes of this paper, we take the plasma sheet and the current-carrying region to be the same.

Coordinate System Used: The positive x-axis points away from the earth. The positive y-axis points toward dawn and the positive z-axis points northward.

## 2. THE PLASMA SHEET

The plasma sheet is considered to be a dynamic, turbulent medium. The dynamic components average out over long periods of time to steady-state values. However, over shorter time-scales the dynamic behavior has profound effects. First, we examine the steady-state component and determine the time-scales of interest. Then a macroscopic time-dependent component is examined and conditioned for its presence deduced.

The Steady-State: The basic steady-state equations are (Spitzer<sup>11</sup>):

$$\nabla P = \frac{j}{c} \times B \quad (1)$$

$$E + v/c \times B = \eta j + \frac{1}{ne} \nabla P_i \quad (2)$$

where  $P$  is the particle pressure,  $\eta$  the resistivity, and  $n$  the particle number density.

The current density required to maintain (1) can be obtained simply by taking the cross product of  $B$

10. Garrett, H.B. (1973) ULF magnetic fluctuations in the plasma sheet as recorded by the Explorer 34 satellite, *J. Geophys. Res.* 78:3799.

11. Spitzer, Lyman, Jr. (1956) *Physics of Fully Ionized Gases*, Interscience Publ.



$$\mathbf{j} = c \frac{\mathbf{B} \times \nabla P}{B^2} \quad (3)$$

We assume the B-field components inside the plasma sheet to be

$$B_z = B_y = 0$$

and

$$B_x = \frac{-2 B_0 z}{l} \quad (4)$$

The latter is based on the measurements of Bowling and Wolf.<sup>9</sup> Here  $B_0$  is the x magnetic field intensity in the tail lobes and  $l$  the thickness of the plasma sheet in the z direction. Equation (1) can be written in the more usual form

$$\nabla P = -\nabla \left( \frac{B^2}{8\pi} \right) \quad (5)$$

Inserting (5) into (3) using (4) yields

$$j_y = -\frac{c B_0}{2\pi l} \quad (6)$$

which, of course, can be directly obtained from the Biot-Savart law.

From (1) and (2), the resistivity is near the neutral sheet

$$\eta = E_y / j_y = \frac{m_i \nu}{ne^2} \quad (7)$$

Here  $\nu$  is the collision frequency and  $m_i$  instead of  $m_e$  is used because protons carry most of the current (Hones et al<sup>12</sup>).

The resistivity, therefore, is a sensitive measure of proton scattering by turbulence (Akhiezer et al<sup>13</sup>). For illustrations we choose  $B_0 = 10\gamma$ ,  $n = 0.3 \text{ cm}^{-3}$ ,  $l = 2.3 R_e$  and  $E_y \sim 10^{-5}$  volts/m. Under these quiet-time conditions

12. Hones, Jr., E.W., Bame, S.J., and Asbridge, J.R. (1976) Proton flow measurements in the magnetotail plasma sheet made with Imp 6, J. Geophys. Res. 81:227.
13. Akhiezer, A.I., and Akhiezer, I.A. (1975) Plasma Electrodynamics Volume 2: Non-linear Theory and Fluctuations, Pergamon Press, Inc., New York.



$$j_y = 1 \text{ na/m}^2$$

$$\nu \simeq 0.04 \text{ collisions/sec} \quad (8)$$

$$\tau = 1/\nu = 25 \text{ sec}$$

For comparable disturbed conditions we take  $B_0 \simeq 10\gamma$ ,  $n \simeq 0.3 \text{ cm}^{-3}$ ,  $l \simeq 1500 \text{ km}$  and  $E_y \simeq 2 \times 10^{-3} \text{ V/m}$ . In this case

$$j_y = 10.6 \text{ na/m}^2$$

$$\nu \simeq 0.9 \text{ collisions/sec} \quad (9)$$

$$\tau = 1/\nu = 1.1 \text{ sec}$$

Equations (8) and (9) give time-scales within which a coherent time-dependent component can exist before being dissipated by turbulence. The effective electron-ion collision frequency associated with ion-acoustic turbulence is  $\sim 0.4 T_e/T_i$  (Biskamp<sup>14</sup>) for the disturbed conditions given above. This is on the same order as (9).

Time-Dependent Behavior: In Appendix A we have solved the Lorentz equation exactly in the limit of zero electric field. This limit is considered appropriate since E-field acceleration should be small between individual collisions. The exact solutions take the form of Jacobi elliptic functions which are well defined in standard texts of Mathematical Physics. As shown in Appendix A and Figure A1, the topology of individual particle trajectories is dependent on the numerical value of the modulus associated with the Jacobi functions. The particle energy ( $E_{cp}$ ) that corresponds to the modulus-squared equal to one divides particle trajectories into two main groups; those of lower energy that do not cross the neutral sheet and those of higher energy that do. The critical energy,  $E_{cp}$ , for particles that have their turning points on the plasma sheet boundaries is given by

$$E_{cp} = \frac{m}{128} \omega_c^2 l^2 \quad (10)$$

14. Biskamp, D. (1973) Collisionless shock waves in plasmas, Nucl. Fusion 13:719.

where  $\omega_c = e B_0 / mc$  is the gyrofrequency and  $m$  the particles mass. In Appendix A it is shown that for protons  $E_{cp} \gg kT$  when  $l \simeq 2.3 R_e$ ,  $kT = 2$  keV and that  $E_{cp} \ll kT$  when  $l \simeq 1500$  km. In other words, the Lorentz equation predicts that the majority of protons will follow trajectories as shown in Figure A1d. rather than those in Figure A1a. as the plasma sheet is compressed. The trajectory shown in Figure A1d. is harmonic and it is the turning on and off of this harmonic motion as the plasma sheet contracts and expands that regulates substorm activity.

The periodicity of the north-south proton motion is directly found by setting the first argument in the Jacobi function  $cn$  (see Eq. (A7)) to  $4K$ . (This particular Jacobi function has, by definition, a period of  $4K$  in the first argument.) Here  $K$  is the complete elliptic integral of the first kind. The result is

$$\tau = \frac{2K(k)}{\left(\frac{\omega_c V}{2l}\right)^{1/2}} \quad (11)$$

where  $V$  is the proton's velocity,  $k^2 = z_m^2 \omega_c / 2Vl$  and  $z_m$  = the distance of the particle's turning point from the neutral sheet. The complete elliptic integral of the first kind becomes singular as  $k^2 \rightarrow 1$ , which corresponds to the case shown in Figure A1b.

Now let us develop an equivalent fluid representation of the single-particle motion shown in Figure A1d. In the cold plasma limit and in the absence of bulk flow the fluid equation of motion is

$$\rho \frac{\partial \dot{z}}{\partial t} = \frac{1}{c} \dot{z} \times \underline{B} = -\nabla \left( \frac{B^2}{8\pi} \right) \quad (12)$$

This equation implicitly assumes that the cold protons are the sole source of  $\underline{B}$ . For the field specified in Eq. (4), Eq. (12) also reduces to that of a harmonic oscillator

$$\rho \ddot{z} = -\frac{B_0^2}{\pi l^2} z = -\omega^2 z \quad (13)$$

where

$$\omega = \frac{2}{l} V_A$$

$$V_A = B_0 / \sqrt{4\pi\rho} \quad (14)$$

The solution for a fluid element starting at  $z = z_m$  with zero initial velocity in the Z-direction is

$$z = z_m \cos \omega t \quad (15)$$

If Eq. (14) is to represent the same dynamics as Eq. (11), then a correction term must be applied to account for the singular behavior of K. This correction term is

$$\omega' = \frac{\pi\omega}{2K(k)} \quad (16)$$

such that  $\omega' \rightarrow \omega$ ,  $K \rightarrow \pi/2$ , as  $k \rightarrow 0$ . The case  $k \rightarrow 0$  is the large velocity limit. The condition that Eq. (16) is an alternate fluid representation of the single-proton harmonic motion shown in Eq. (11) is

$$T' = 2\pi/\omega' = \tau \quad (17)$$

which reduces to

$$j = nev = cB_0/2\pi l \quad (18)$$

Equation (18) may be stated in terms of a theorem. If the current density in the plasma sheet is taken as  $nev$  where  $n$  is the proton number density and  $v$  the total mean velocity in the Z - Y, plane then the time-dependent cold plasma equation of motion will be that of an oscillator with a period in the Z (north-south) direction which is equivalent to that obtained by an exact solution of the Lorentz equation. The physical picture of an ensemble of protons moving with random phase throughout the plasma sheet can be replaced by a continuum or field of independent harmonic oscillators (Henley and Thirring<sup>15</sup>) as defined by the cold plasma Eq. (13). This is the equivalent, time-dependent fluid representation of the single-particle motion in phase space. When averaged over a surface element, both treatments lead to the same result since they have identical dynamical properties.

The physical significance of the cold plasma approach can be considered as follows: Introduce a finite collision frequency into the above treatment. Over long time periods the single particle motion will be averaged or washed out by collisions. However, let us consider shorter time scales. The number of expected collisions over a given time scale follows Poisson statistics so that the number of protons

15. Henley, E.M., and Thirring, W. (1962) Elementary Quantum Field Theory, McGraw-Hill Book Co., Inc.



that do not collide increases exponentially as the time interval decreases. Eventually, one reaches a limit where the cold plasma equations are valid. In the present case, the cold equations need only be valid over the time interval required for a proton to cross the plasma sheet in the z-direction. For  $B_0 = 30 \gamma$ ,  $l = 1500$  km,  $E = 5.0$  keV this is  $\sim 2$  sec (Eq. (11)) which is comparable to the estimated mean collision time of  $\sim 1$  sec (Eq. (9)).

The protons in this picture can be considered test particles (Akhiezer and Akhiezer<sup>13</sup>) that are scattered by plasma fluctuations generated by collective phenomenon. The combined effects of all such generated phenomena is incorporated in the numerical value of the collision frequency,  $\nu$ . A finite  $\nu$  introduces a Langevin collision term on the right-hand side of the Boltzmann equation which implies a net momentum transfer from protons to electrons via plasma fluctuations. With such a term, Eq. (13) becomes the well-known equation for a damped oscillator. Thus, the importance of single particle motion in controlling the dynamics of the tail is modulated by the degree of plasma turbulence generated by instabilities. In Section 4 we show that for critical damping ( $\omega = \nu/2$ ), there will be a rapid heating of electrons near the neutral sheet at a rate  $\sim (B_0^2/8\pi)V_A$ .

We now derive a simple criteria for the presence of the harmonic motion across the neutral sheet. Consider the particles as having two independent oscillatory modes: one being the usual gyromotion represented by  $\omega_c$ , and the other being the north-south harmonic motion represented by  $\omega$ . The north-south component will dominate when

$$\omega \geq \bar{\omega} = 1/2 \omega_c \quad (19)$$

which reduces to

$$n l^2 \leq 8.15 \times 10^{15} \text{ proton/cm} \quad (20)$$

For a nominal density of  $0.3 \text{ cm}^{-3}$

$$l \leq 1634 \text{ km}$$

As in the single-particle treatment, a decrease in  $l$  is required to trigger the north-south harmonic motion. Based on the above, we use  $\sim 1500$  km as a nominal value for the plasma sheet thickness during onsets.

Equilibrium Distribution of the Harmonic Component: The time-dependent component, because of its oscillator properties, can lead to a steady-state distribution. For any oscillator one may eliminate the independent variable  $t$  from

the  $(z, \dot{z})$  equations. Then an observer at coordinate point  $z$  will measure a density  $n(z, z_m)$  from protons originating at  $z_m$ . That is:

$$\bar{n}(z, z_m) = \frac{\text{const.}}{\dot{z}} = \frac{\text{const.}}{\omega(z_m^2 - z^2)^{1/2}} \quad (21)$$

Now only protons with turning points greater than  $z$  can pass through  $z$ . Therefore,

$$n'(z) = \int_z^{l/2} \bar{n}(z, z_m) dz_m = \frac{\text{const.}}{\omega} \left( \frac{l^2}{4} - z^2 \right)^{1/2} \quad (22)$$

$$\int_0^{l/2} n'(z) dz = \alpha n l / 2$$

where  $\omega$  is defined in (14). This leads to an enhanced density at  $z = 0$  relative to that at  $z = \pm l/2$ . The integration of  $n'$  over  $z$  from 0 to  $l/2$  determines the constant. This constant is equal to  $4\alpha n\omega/l\pi$  where  $n \approx 0.3 \text{ cm}^{-3}$  and  $\alpha$  is defined by (24).

Multiple Onsets: Consider a localized impulse imparted to the external boundary of the north tail lobe. This impulse will propagate through the tail lobe via a compressional wave as described in Section 4. Upon reaching the plasma sheet boundary, it will impart additional energy to protons just turning at the interface (see Figure A1d.). These protons will, if not scattered, transfer the impulse to the opposite tail lobe boundary. The presence of the north-south harmonic motion, therefore, will dynamically couple the two lobes and the entire tail will respond as a unit. Any slowing down or scattering of the coherent protons would, of course, prevent them reaching the opposite boundary and, hence, the coupling would be broken.

The probability that a proton will not suffer a collision during a time interval,  $t$ , is given by the Poisson distribution,

$$\rho(0, \nu t) = e^{-\nu t} \quad (23)$$

Returning to the fluid picture where the harmonic motion is represented by a field or continuum of independent oscillators the fractional number of these oscillators that are undamped during a half-period is given by  $e^{-\pi\nu/\omega'}$ . The effective



oscillator strength of the plasma sheet in terms of ability to coherently transfer information from one boundary to the other is therefore given by

$$K_F = \omega_i^2 e^{-\pi\nu/\omega_i} = \alpha\omega_i^2 \quad (24)$$

The parameter,  $K_F$ , is the equivalent spring constant of the plasma sheet. In Section 4 an equivalent constant will be derived for the tail lobes. The eigenmodes of such a system are then examined in terms of multiple onsets. The periodicity of the onsets is modulated by  $\nu$  through Eq. (24).

But first in Section 3 we derive a theory for merging based on magnetic instabilities that are generated by localized currents. These localized currents are presumed generated by particle motion such as shown in Figure A1b. This motion is also significant when the plasma sheet is sufficiently compressed.

### 3. MERGING

In the previous section, it was shown that a transverse harmonic component can exist if the plasma sheet is sufficiently compressed. In the present section, we derive a theory showing it is possible to have direct field line merging if the magnetic instabilities are large enough. This direct merging is advanced as an explanation for the sporadic reconnection at maximum compression reported by Pytte et al.<sup>1</sup> Energy conservation is also discussed.

What is meant by direct merging is shown in Figure 1. A localized current fluctuation causes deformation of the field lines on the plasma sheet boundaries. As these field lines convect into the plasma sheet they become statically unstable. It is argued that if (19) is satisfied then the motion of the attached electrons can cause these field lines to uniformly and smoothly connect across the x-axis and merge into two separate field lines. Criteria for this process to occur is derived.

This problem is approached by determining consistency conditions on the deformation itself. The corresponding B-field inside the plasma sheet is then derived. We assume that in the vicinity of the deformation that B is a weak function of Z. That is:

$$\frac{\partial B_x}{\partial z} \simeq \frac{\partial B_z}{\partial z} \simeq 0 \quad (25)$$

which implies from the constraint  $\nabla \cdot B = 0$  that

$$\frac{\partial B_x}{\partial x} = 0 \text{ or } B_x = \text{const.} \equiv -B_0 \quad (26)$$



The  $z$ -component is then determined directly from the slope of the deformation

$$B_z = -B_0 f'(x) \quad (27)$$

Equations (26) and (27) represent the simplest form for a  $B$ -field line next to that for a uniform field. We now build a theory assuming that (26) and (27) properly describe the deformations. Equation (27) suggests that current fluctuations add  $B$ -field energy to the deformation through the creation of a  $B_z$  component.

## DIRECT MERGING BY CURRENT FLUCTUATIONS

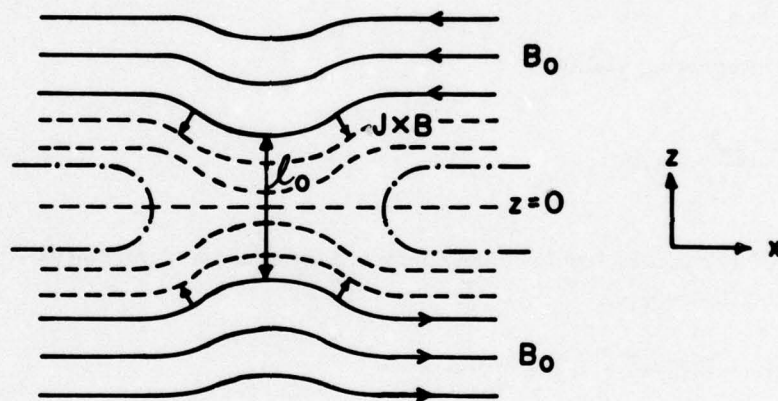


Figure 1. A Schematic Representation of the Earth's Magnetotail. The solid lines show the tail lobe field lines being deformed by a localized interruption of the cross-tail current near  $z = 0$  (see text). The dotted lines represent the connected field lines inside the plasma sheet. Merged field lines are represented by the dash-dot-dash lines

B-field Lines Inside the Plasma Sheet. The stresses acting on the deformation have opposing  $x$ -components (Figure 1). This fact, together with  $B_x(x=0) < B_0$  in the plasma sheet, implies that the convected field lines will continue to deform and stretch. We assume that these field lines will be closely approximated by a family of field lines that (1) join smoothly to the deformation (2) are divergence free and (3) are symmetric about the  $x$ -axis.

The simplest form for  $B_x$  which satisfies the boundary condition at  $z = l(x)/2$  is

$$B_x = -2 \frac{B_0 z}{l(x)}, \quad l(x) = l_0 + 2f(x) \quad (28)$$

where  $l(x)$  is the separation between the plasma sheet boundaries in the region of the deformation. The parameter  $l_0$  denotes the minimum separation at  $x = 0$ . The  $z$ -component of  $B$  is assumed to have the functional form.

$$B_z(x, z) = -B_0 f'(x) g(x, z) \quad (29)$$

where  $g(x, z)$  is to be determined subject to the constraint  $g(z = l(x)/2) = 1$ . Using (28) and (29)  $\nabla \cdot B = 0$  implies

$$g, z = \frac{4z}{l^2} \quad (30)$$

which upon integrating yields

$$g(x, z) = \frac{2z^2}{l^2} + 1/2 \quad (31)$$

The factor of  $1/2$  comes from the boundary condition at the deformation. The  $B_z$  component is, therefore,

$$B_z(x, z) = -[2z^2/l^2 + 1/2] B_0 f'(x) \quad (32)$$

The point is that as  $z \rightarrow 0$ ,  $B_x \rightarrow 0$ , however,  $B_z$  does not vanish at  $z = 0$  but has a spectrum of values depending on the steepness of the deformation. It is argued that the convected field lines originating with deformations on opposite sides of the neutral sheet may join by superposition to form a new family of field-lines; one set earthward and the other tailward of the merging point (see Figure 1).

Merged Field Lines: The simplest form for a merged field (Eastwood<sup>16</sup>) is

$$B_x = -2 B_0 z/l \quad (33)$$

$$B_z = \pm B_{zi} = \text{const.}$$

$$B_y = 0$$

16. Eastwood, J. W. (1973) Consistency of fields and particle motion in the "Speiser" model of the current sheet, Planet. Space Sci. 20:1555.

The shape of the field lines is determined by

$$\frac{dx}{dz} = \frac{2 B_o z}{B_{zi} l} \quad (34)$$

$$x = x_c + \frac{B_o z^2}{B_{zi} l}$$

That is, a parabolic shape about the x-axis. Now in the region of the deformation an analysis similar to (31) is carried out except now the boundary condition on  $B_z$  is

$$B_z(z = 0) = -B_{zi} \quad (35)$$

where  $B_{zi}$  is the residual value of  $B_z$  (Bowling and Wolf,<sup>9</sup> and Behannon<sup>17</sup>). This leads to

$$B_z(x, z) = - \left[ 2B_o f' \frac{z^2}{l^2} + B_{zi} \right] \quad (36)$$

Outside the deformed region where  $f'(x) = 0$  Eq. (36) reduces to (33).

At some point x, Eq. (32) will be indistinguishable from (36) if

$$\frac{B_o f'(x)}{2} = B_{zi} \quad (37)$$

In this case the B-field components of a field line originating on the deformations will be the same as those of a merged field line. Since the values of  $f'$  varies from 0 at the bottom of the deformation to some maximum value,  $f'_m$ , at the inflection point then (37) can be expressed as the inequality.

$$f'_m \geq \frac{2 B_{zi}}{B_o} \quad (38)$$

Let us refer to Figure 2 for the physical implications of this result. Assume there exists a power density spectrum for magnetic fluctuations as a function of  $f'_m$ . This is represented by the curve on the left-hand side of the figure. Quiet

17. Behannon, K. W. (1970) Geometry of the geomagnetic tail, J. Geophys. Res. 74:743.



ASSUMPTION: THERE EXISTS A POWER DENSITY SPECTRUM FOR MAGNETIC FLUCTUATIONS AS A FUNCTION  $f'_M$

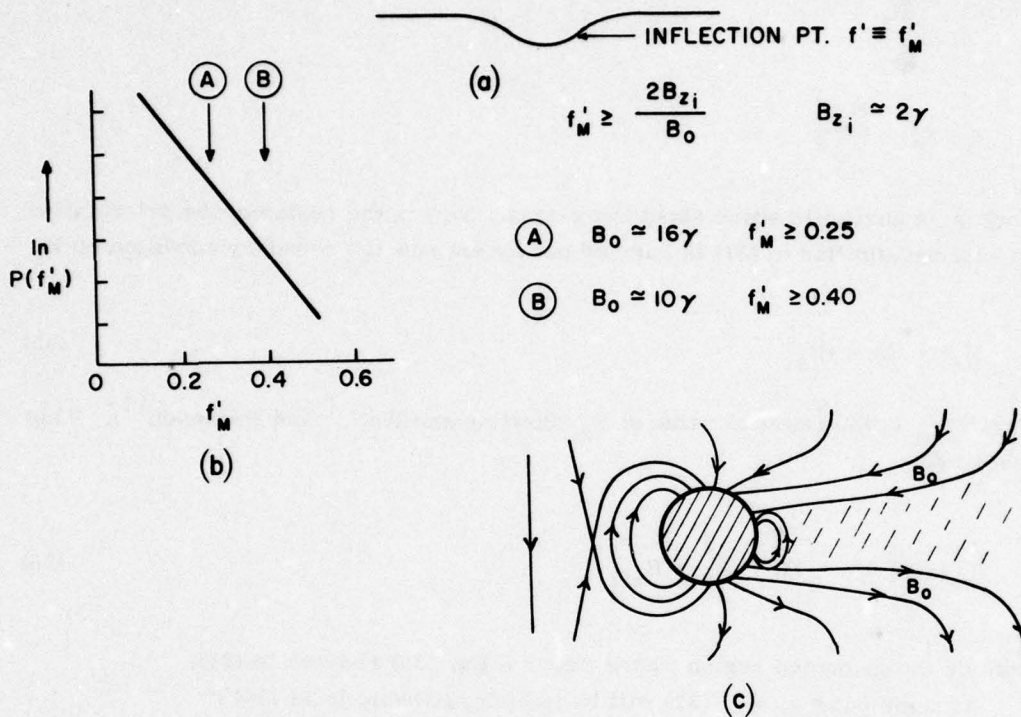


Figure 2. Assumption: There Exists a Power Density Spectrum for Magnetic Fluctuations as a Function  $f'_M$ . (a) A typical magnetic instability (deformation). The maximum slope,  $f'_M$ , is at the inflection point; (b) A hypothetical power spectrum as a function of  $f'_M$ ; (c) An idealized model showing how merging on the day side causes  $B_0$  to increase, thereby decreasing the threshold at which merging occurs

time conditions are represented by point B. As merging increases on the dayside,  $B_0$  increases in the tail lobes, therefore, decreasing the threshold value of  $f'_M$  at which merging can take place. This is denoted by point A. In this manner the nightside merging rate is controlled by the dayside rate. The process is very analogous to a variable threshold discriminator where the threshold is regulated by the dayside merging rate through  $B_0$ . An increase in  $B_{zi}$  would decrease the merging rate, thereby allowing the temporary build-up of magnetic energy in the tail lobes.

**Current Fluctuations:** Taking the curl of the components as defined in expressions (28) and (32), it is found that in the region of the deformation that the current density is

$$j_y(x, z) = -\frac{cB_0}{2\pi l} \left[ 1 + \frac{4z^2}{l^2} f'^2 \right] + \frac{cB_0}{8\pi} f'' \left[ 1 + \frac{4z^2}{l^2} \right] \quad (39)$$

At  $x = 0$ ,  $z = 0$ ,  $f' = 0$  and  $f''(0)$  is equal to the curvature  $K$  of the field line at the boundary so that

$$j_y(0, 0) = -\frac{cB_0}{2\pi l_0} + \frac{cB_0}{8\pi} K \quad (40)$$

The current density is positive if the curvature of the deformation is large enough.

$$K \geq 4/l_0 \quad (41)$$

Alternatively the presence of a positive flowing current implies positive curvature. A positive flowing current fluctuation is supplied by the single particle motion described in Appendix A and in Figure A1b.

**Energy Conservation.** The acceleration of plasma by the relaxation of the merged field lines will now be derived. It is shown that the magnetic energy is converted into plasma kinetic energy. For simplicity, we assume  $B_z = B_{zi}$  throughout the plasma sheet where  $B_z$  points northward earthward of the merging region and southward tailward of the region. The  $B_x$  component is taken as shown in (33). In that case, it was shown that the merged field lines have a parabolic shape. The orthogonal plasma trajectories are determined by

$$\frac{dx}{dz} = -\frac{B_{zi}l}{2B_0 z} \quad (42)$$

which can be integrated and solved for  $z$ .

$$z = z_i \exp \left[ -\frac{2B_0}{B_{zi}l} (x - x_i) \right] \quad (43)$$

The accelerated plasma asymptotically approaches the  $x$ -axis as  $x \rightarrow \infty$ .

Energy conservation requires,

$$\frac{1}{2} \rho (v^2 - v_i^2) = \frac{1}{c} \int_{x_i, z_i}^{x, z} (j_y \times B) \cdot ds_{\perp} \quad (44)$$

where i-subscripts denote initial values and  $ds_{\perp}$  is the element of length perpendicular to B. Now

$$j_y = -\frac{cB_0}{2\pi l} \quad (l = \text{const.})$$

$$B = \left( B_{zi}^2 + 4B_0^2 \frac{z^2}{l^2} \right)^{1/2} \quad (45)$$

$$ds_{\perp} = -\frac{B}{B_x} dz \quad (46)$$

Inserting the defined variables from (45) and (46) into (44), one finds

$$\frac{1}{2} \rho (v^2 - v_i^2) = -\frac{B_x^2}{8\pi} \Big|_{x_i, z_i}^{x, z} - \frac{B_{zi}^2}{4\pi} \ln z/z_i \quad (47)$$

Using (43), we find the second term on the R. H. S. is equal to

$$\frac{1}{c} j_y B_{zi} (x - x_i) \quad (48)$$

which is interpreted as work performed by the current in moving the particles from  $(x_i, z_i)$  to  $(x, z)$ . Here  $j_y$  is the unperturbed current. In the limit  $x \rightarrow \infty$ ,  $z \rightarrow 0$  by (43) and  $B_x \rightarrow 0$  (33). Eq. (47) becomes

$$\frac{1}{2} \rho v^2 = \frac{1}{2} \rho v_d^2 + B_0^2/8\pi + \frac{1}{c} j_y B_{zi} (x - x_i) \quad (49)$$

We have replaced  $B_x(x_i, z_i)$  by  $B_0$  since we have shown that in the merging region the  $B_x$  field energy becomes converted into particle kinetic energy.



#### 4. MAGNETOTAIL OSCILLATIONS

Multiple onsets are a distinctive feature of magnetospheric substorms (Pytte et al<sup>1</sup>). In this section, a theory is derived to explain the observed intervals between onsets. This theory predicts a proton collision frequency consistent with (9). Thermal heating of the plasma sheet is also discussed.

It was shown in Section 2 that a substorm onset could lead to harmonic particle motion in the plasma sheet near the region of maximum compression. We now argue that this motion couples to the tail lobes causing the tail to respond as a complete system.

Compression of the tail magnetic field generates transverse compressional waves across the tail lobes that obey the equation (Spitzer<sup>11</sup>).

$$\nabla^2 E_y = \left( \frac{1}{V_A^2} + \frac{1}{c^2} \right) \frac{\partial^2 E_y}{\partial t^2} \quad (50)$$

$$\approx \frac{1}{V_A^2} \frac{\partial^2 E_y}{\partial t^2}$$

where  $V_A$  is again the Alfvén velocity. Now

$$\dot{z} = c E_y / B_0 = \frac{c}{B_0} E_0 e^{i(kz - \omega t)} \quad (51)$$

so that

$$\ddot{z} = -k^2 V_A^2 \dot{z} \quad (52)$$

where  $k$  is the wave vector. This reduces upon integration to

$$\ddot{z} = -k^2 V_A^2 z \quad (53)$$

which is again the equation for a harmonic oscillator. The reduction of the wave equation to that of a harmonic oscillator is well known (Henley and Thirring<sup>15</sup>). Equation (53) determines the equivalent force constant,  $K_A$ , in the tail lobes.

$$K_A = k^2 V_A^2 \quad (54)$$

The wave-vector,  $k$ , will only have certain discrete values if the tail lobes act as wave-guides (McClay and Radoski<sup>18</sup>). If  $r_o$  is the height of the tail lobe in the  $z$ -direction, then the compressional wave will reflect at the plasma sheet boundary and return to the outer surface after a time,  $t$ , where

$$t = \frac{2r_o}{V_A} = \frac{2\pi}{\omega_A} \quad (55)$$

or

$$\omega_A = \frac{\pi}{r_o} V_A \quad (56)$$

Now since

$$\omega_A = k V_A \quad (57)$$

(56) and (57) lead to

$$k = N \frac{\pi}{r_o} \quad (58)$$

where  $N$  is a positive integer. This simplified derivation leads to results identical to those obtained from more sophisticated approaches (McClay and Radoski<sup>18</sup>). Inserting (58) into (54), we have

$$K_A = \frac{N^2 \pi^2}{r_o^2} V_A^2 \quad (59)$$

The continual compression of the tail lobes by the solar wind ensures that the natural frequencies represented (59) will always be present.

Now the oscillator strength in the plasma sheet as taken from Section 2 is

$$K_F = \alpha \frac{4}{l^2} V_A^2 \quad (60)$$

18. McClay, J. F., and Radoski, H. R. (1967) Hydromagnetic propagation in a theta-model geomagnetic tail, J. Geophys. Res. 72:4525.

The parameter  $\alpha$  is a direct measure of the turbulence in the plasma sheet where a small value of  $\alpha$  implies a highly turbulent medium (that is, a high collision frequency). The turbulent component does not transfer coherent momentum from one tail lobe to another. The same values for  $B_0$ ,  $\rho$  and  $r_0$  are assumed in both tail lobes so that one has three harmonic oscillators strung in a line, with the outer two oscillators having identical force constants. Figure 3 shows the conceived arrangement. This system is now solved in the limit of small amplitude oscillations in Appendix B.

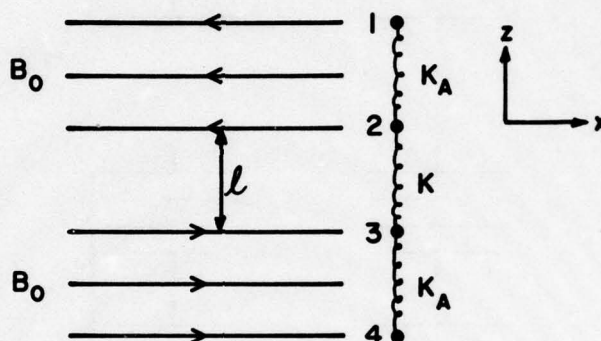


Figure 3. The Magnetotail Modeled as Three Coupled Oscillators.  $K_A$  is determined from the eigenmodes of transverse compressional waves in the lobes. The current-carrying region is defined by  $l$

Figure 4 shows the resulting eigenmodes. The first two modes correspond to translation of the plasma sheet without involving any compression or expansion. The last two modes do, however, involve compression and expansion of the plasma sheet. For  $n = 10^{-3} \text{ cm}^{-3}$ ,  $B_0 = 10 \gamma$ ,  $r_0 = 20 R_e$  and with the assumption  $K_F \ll K_A$  the positive root of (B8) becomes using (59)

$$\omega_3 \approx \sqrt{2K_A} \approx 0.24 N \text{ rad/sec} \quad (61)$$

or

$$T_3 = 26/N \text{ sec} \quad (62)$$

Garrett<sup>19</sup> noted an oscillatory-type magnetic fluctuation in the plasma sheet with a period on the order of 50 sec.

19. Garrett, H.B. (1972) ULF Magnetic Fluctuations in the Plasma Sheet as Recorded by the Explorer 34 Satellite, Masters Thesis, Rice University.



# EIGENMODES OF THE COUPLED OSCILLATOR MODEL

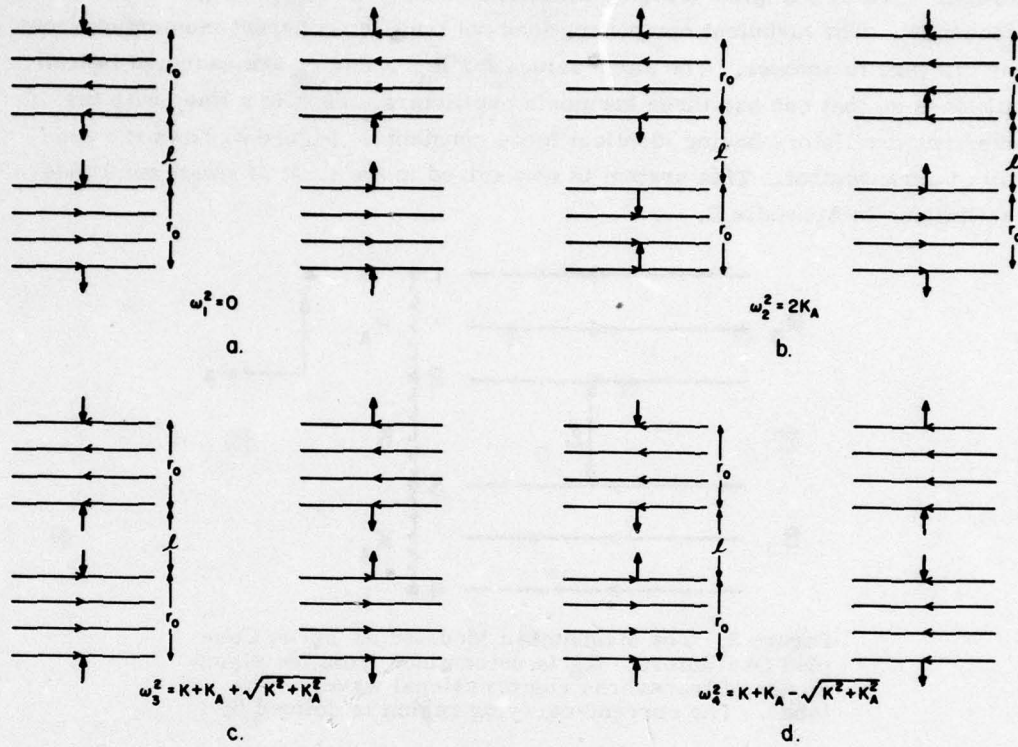


Figure 4. The Four Possible Eigenmodes of the Coupled Oscillator System Shown in Figure 3

The fourth eigenmode shown in Figure 4 is the most interesting since it corresponds to both tail lobes moving toward  $z = 0$ . It is this mode that one expects to be excited by the initial compression of the plasma sheet. The associated eigenfrequency is the negative root of (B8) which goes to zero in the limit  $K_F \rightarrow 0$  and is a measure of the plasma sheet's compressibility compared with that of the tail lobes.

This fact can be seen more clearly, if one solves for  $K_F$  in terms of the eigenfrequency  $\omega_4$ .

$$K_F = \frac{\omega_4^2}{2} \frac{(\omega_4^2 - 2K_A)}{(\omega_4^2 - K_A)} \quad (63)$$

Now the average period between onsets as given by Pytte et al<sup>1</sup> is 12.5 min or

$$\omega_4 = 0.008 \text{ rad/sec} \quad (64)$$

The value of  $K_A$  using the above values for the tail lobe parameters is 0.029 so that the conditions  $K_A \gg \omega_4^2$  is well satisfied. This simplifies (63) to

$$K_F = \omega_4^2 \quad (65)$$

Equating this result to (24) allows the mean proton collision frequency to be solved in terms of  $\omega_4$  and  $\omega'$  (Eq. (16))

$$\nu = -\frac{\omega'}{\pi} \ln \left[ \left( \frac{\omega_4}{\omega'} \right)^2 \right] \quad (66)$$

A Consistency Test: The plasma sheet is assumed to have the same representative values as used for Eq. (9) with  $kT = 2$  kev. This makes  $\omega' = 0.49$  rad/sec. Using (64) for  $\omega_4$ ,  $\nu$  takes on the value of

$$\nu = 1.27 \text{ collisions/sec} \quad (67)$$

from (66) which is in excellent agreement with (9). Note that (67) was derived from the period between onsets while (9) was derived from the resistivity relation. This indicates an overall consistency of the theory as described in Sections 2 and 4.

Taking  $\nu$  on the order of one collision per second then  $\alpha$  (see Eq. (16)) is equal to 0.1 percent. Recall that  $\alpha$  is the fraction of protons that execute at least one period before being diverted by collisions. This is verification of the original hypothesis that the harmonic component is a small fraction of the turbulent plasma medium but plays an extremely important role in terms of the plasma sheet dynamics.

Thermal Heating of the Plasma Sheet: We have seen that a very small fraction of protons contribute to the coupling of the plasma sheet to the tail lobes. What about the other protons that are more rapidly thermalized?

It is well known that for a damped oscillator that the frequency for critical damping is given by  $\omega_0 = \nu/2$ . Note that in the present case  $\omega_0 = 0.53$  rad/sec and  $\nu \simeq 1$  collision/sec which quantitatively consistent with critical damping. The rate at which energy is being thermalized is, therefore, given by

$$\frac{dE}{dt} = -\rho \dot{z}^2 \nu \quad (68)$$

per unit volume. The general solution for the critically damped case is

$$z = z_m (1 + \nu t/2) e^{-\nu/2 t} \quad (69)$$

where the initial conditions  $z = z_m$ ,  $\dot{z} = 0$  at  $t = 0$  have been used. Equation (69) can be differentiated to obtain

$$\dot{z} = -\omega_o^2 z_m t e^{-\nu/2 t} \quad (70)$$

which when inserted into (68) and time-averaged over a quarter-cycle ( $t = \pi/2\omega_o$ ) gives

$$\left\langle \frac{dE}{dt} \right\rangle = -\frac{\rho \omega_o^3 z_m^2}{\pi} \left[ 1 - e^{-\pi} \left( 1 + \pi + \frac{\pi^2}{2} \right) \right] \quad (71)$$

The contribution from all elements from  $z_m = 0$  to  $z_m = l/2$  is included by integration.

$$\left\langle \frac{d\epsilon_{tot}}{dt} \right\rangle = -\frac{\rho \omega_o^3 l^3 (0.61)}{24\pi} \quad (72)$$

Inserting  $\omega_o = 2/l V_A$  into (72) gives the final result.

$$\left\langle \frac{d\epsilon_{tot}}{dt} \right\rangle \sim -\frac{2}{3\pi} \left( \frac{B_o^2}{8\pi} \right) V_A \quad (73)$$

which is the rate of thermal heating per square centimeter. Multiplying by the length and width of the tail over which heating is taking place gives the total power input for one hemisphere. The damping of the  $J \times B$  motion by collisions heats the plasma sheet at a rate which is comparable to that expected if magnetic energy was being annihilated at the Alfvén speed.

Consider the analogous case of an electric motor in a viscous medium where an external "battery" supplies the power to drive the armature. In the same manner the source of the cross tail electric field supplies the power that heats the plasma sheet by the above process. Note, however, that the rate of heating goes as  $B_o^3$  and, therefore, is controlled by the dayside merging rate. Heating by collisional damping by the  $J \times B$  force will exceed joule heating if  $B_o > 22\gamma$  and the parameter values given in Eq. (9) are retained.



## 5. SUMMARY AND CONCLUSIONS

In this model, we found that when the plasma sheet is compressed harmonic motion across the plasma sheet is enhanced. This is true for both the fluid and particle treatments. This harmonic component dynamically couples the plasma sheet to the tail lobes and acts as a substorm triggering mechanism. The characteristic frequency of the oscillation mode determines the period between onsets which is a sensitive measure of the mean proton collision frequency,  $\nu$ , in the plasma sheet. Consistency was found between the collision frequency obtained from the onset period and from the resistivity equation.

In the fluid approximation the plasma sheet can also be thermally heated under compression in a manner analogous to that of a critically damped oscillator. This occurs when  $t \simeq 4 V_A / \nu$ .

Current fluctuations that arise from changes in single particle motion are considered to drive B-field fluctuations. These B-field fluctuations can merge by superposition if the corresponding deformation is severe enough and if merging is taking place on the dayside. Subsequent relaxation of the merged lines accelerates particles parallel to B.

We conclude that the above ideas provide a useful and viable model for the onset of magnetospheric substorms.

## References

1. Pytte, T., McPherron, R.L., Kivelson, M.G., West, Jr., H.I., and Hones, Jr., E.W. (1976) Multiple-satellite studies of magnetospheric substorms: radial dynamics of the plasma sheet, J. Geophys. Res. 81:5921.
2. Alfvén, H. (1968) Some properties of magnetospheric neutral surfaces, J. Geophys. Res. 73:4379.
3. Dessler, A.J. (1971) Vacuum merging: a possible source of the magnetospheric crosstail electric field, J. Geophys. Res. 76:3174.
4. Sweet, P.A. (1958) The neutral point theory of solar flares, in Electromagnetic Phenomena in Cosmical Physics, Ed., by B. Lehnert, p. 123, Cambridge University Press, London.
5. Parker, E.N. (1963) The solar-flare phenomenon and the theory of reconnection and annihilation of magnetic fields, Astrophys. J. Suppl. Ser. 8:177.
6. Coppi, B. and Friedland, A.B. (1971) The processes of magnetic-energy conversion and solar flares, The Astrophys. J. 169:379.
7. Vasylunas, V.M. (1975) Theoretical models of magnetic field line merging, 1, Rev. of Geophys. and Space Phys. 13:303.
8. Petschek, H.E. (1964) Magnetic Field Annihilation AAS-NASA Symposium on the Physics of Solar Flares, NASA Spec. Publ. SP-50, 425.
9. Bowling, S.B., and Wolf, R.A. (1974) The motion and magnetic structure of the plasma sheet near  $30 R_E$ , Planet. Space Sci. 22:673.
10. Garrett, H.B. (1973) ULF magnetic fluctuations in the plasma sheet as recorded by the Explorer 34 satellite, J. Geophys. Res. 78:3799.
11. Spitzer, Lyman, Jr. (1956) Physics of Fully Ionized Gases, Interscience Publ.
12. Hones, Jr., E.W., Bame, S.J., and Asbridge, J.R. (1976) Proton flow measurements in the magnetotail plasma sheet made with Imp 6, J. Geophys. Res. 81:227.

13. Akhiezer, A.I., and Akhiezer, I.A. (1975) Plasma Electrodynamics Volume 2: Non-linear Theory and Fluctuations, Pergamon Press, Inc., New York.
14. Biskamp, D. (1973) Collisionless shock waves in plasmas, Nucl. Fusion 13:719.
15. Henley, E.M., and Thirring, W. (1962) Elementary Quantum Field Theory, McGraw-Hill Book Co., Inc.
16. Eastwood, J.W. (1973) Consistency of fields and particle motion in the "Speiser" model of the current sheet, Planet. Space Sci. 20:1555.
17. Behannon, K.W. (1970) Geometry of the geomagnetic tail, J. Geophys. Res. 75:743.
18. McClay, J.F., and Radoski, H.R. (1967) Hydromagnetic propagation in a theta-model geomagnetic tail, J. Geophys. Res. 72:4525.
19. Garrett, H.B. (1972) ULF Magnetic Fluctuations in the Plasma Sheet as Recorded by the Explorer 34 Satellite, Masters Thesis, Rice University.



## Bibliography

- Akasofu, S. -I. (1976) Physics of Magnetospheric Substorms, D. Reidel, Dordrecht-Holland.
- Baker, D.N., and Stone, E.C. (1977) Observations of energetic electrons ( $E \geq 200$  kev) in the earth's magnetotail: plasma sheet and fireball observations, J. Geophys. Res. 82:1532.
- Cowling, T.G. (1957) Magnetohydrodynamics, Interscience Publ., New York.
- Frank, L.A., Ackerson, K.L. and Lepping, R.P. (1976) On hot tenuous plasmas, fireballs, and boundary layers in the earth's magnetotail, J. Geophys. Res. 81:5859.

## Appendix A

### Single Particle Trajectories

In this appendix, single particle motion in the plasma sheet is examined. The equations of motion (Speiser<sup>1</sup>) in the present system of coordinates is

$$\ddot{x} = 0$$

$$\ddot{y} = -\frac{2eB_0}{lmc} z \dot{z} - \frac{eE}{m} \quad (A1)$$

$$\ddot{z} = \frac{2eB_0}{lmc} z \dot{y}$$

These hold for a linear  $z$ -dependence in  $B_x$ . By integration and substitution (A1) can be rewritten (Speiser<sup>1</sup>) as

$$\dot{y} - \dot{y}_0 = \frac{-eB_0}{lmc} (z^2 - z_0^2) - \frac{eE}{m} t \quad (A2)$$

$$\ddot{z} = \frac{2eB_0}{lmc} z \left[ -\frac{eB_0}{lmc} (z^2 - z_0^2) - \frac{eE}{m} t + \dot{y}_0 \right]$$

1. Speiser, T.W. (1965) Particle trajectories in model current sheets, 1, Analytic solutions, J. Geophys. Res. 70:4219.

The case for long times was treated extensively by Speiser.<sup>1</sup> In this limit

$$\ddot{z} \approx - \frac{2e^2 E B_0 t}{l m^2 c} z = -\omega^2 z \quad (A3)$$

which is the equation for an oscillator with a time-dependent frequency. For completeness, the numerical value of  $\omega$  is

$$\omega = 0.50 \sqrt{t} \text{ rad/sec} \quad (A4)$$

where  $B_0 = 10 \gamma$ ,  $E = 2 \text{ mv/m}$  and  $l = 1500 \text{ km}$ . This is analogous to the fluid result in Section 2 of the front text.

In the alternate limit of zero electric field the limit (A3) does not exist and (A1) reduces to

$$\ddot{y} = - \frac{2eB_0}{lmc} z \dot{z} \quad (A5)$$

$$\ddot{z} = \frac{2eB_0}{lmc} z \dot{y}$$

By defining

$$k^2 = \frac{z_m^2 e B_0}{2 v l m c} \quad (A6)$$

(A5) can be directly solved in terms of elliptic integrals and functions (Byrd and Friedman<sup>2</sup>) for three cases of interest.

Case I:

$$k^2 < 1$$

$$y = - \frac{z_m}{k} E \left( \frac{2kvt}{z_m} \right) + vt \quad (A7)$$

$$z = \pm z_m \text{ cn} \left( \frac{2kvt}{z_m}, k \right)$$

2. Byrd, P. F. and Friedman, M. D. (1954) Handbook of Elliptic Integrals for Engineers and Physicists, Springer-Verlag Publ., Berlin.



Case II:

$$k^2 = 1$$

$$y = -z_m \tanh \left( \frac{2vt}{z_m} \right) + vt \quad (A8)$$

$$Z = \frac{\pm z_m}{\cosh \left( \frac{2vt}{z_m} \right)}$$

Case III:

$$k^2 > 1$$

$$y = -z_m E \left( \frac{2k^2 vt}{z_m} \right) + 2k^2 vt - vt \quad (A9)$$

$$z = \pm z_m \operatorname{dn} \left( \frac{2k^2 vt}{z_m}, \frac{1}{k} \right)$$

The expressions  $\operatorname{cn}$  and  $\operatorname{dn}$  are Jacobi elliptic functions.  $E(u)$  is the incomplete elliptic integral of the second kind. The constants of integration were chosen so that  $y$  and  $t$  equal zero when  $z = \pm z_m$ .

The  $z$ -coordinate has the following possible values

Case I:

$$-z_m \leq z \leq z_m$$

Case II:

$$-z_m \leq z < 0 \quad \text{or} \quad 0 < z \leq z_m \quad (A10)$$

Case III:

$$-z_m \leq z \leq -\sqrt{1 - \frac{1}{k^2}}$$

or

$$\sqrt{1 - \frac{1}{k^2}} z_m \leq z \leq z_m$$

Note that protons can cross the  $z = 0$  axis only for Case I ( $k^2 < 1$ ). See Figure A1. The parameter  $k^2$  is inversely proportional to the total particle velocity  $v$ . Therefore, Case III corresponds to low energy protons that gyrate solely on one side of the  $z = 0$  axis (Figure A1a). Case II corresponds to protons that start at  $Z = \pm Z_m$  and asymptotically approach  $z = 0$  as  $t \rightarrow \infty$  (Figure A1b). Note that in this case the proton is traveling in the  $+y$  direction at the total velocity. Case I corresponds to protons starting at  $\pm z_m$  with sufficient energy to cross  $z = 0$  (Figures A1c and A1d).

POSSIBLE PROTON TRAJECTORIES IN THE PLASMA SHEET FOR PROTONS  
PASSING THROUGH  $Z_m = 750\text{ km}$   $B_0 = 10\gamma$   $I = 1500\text{ km}$

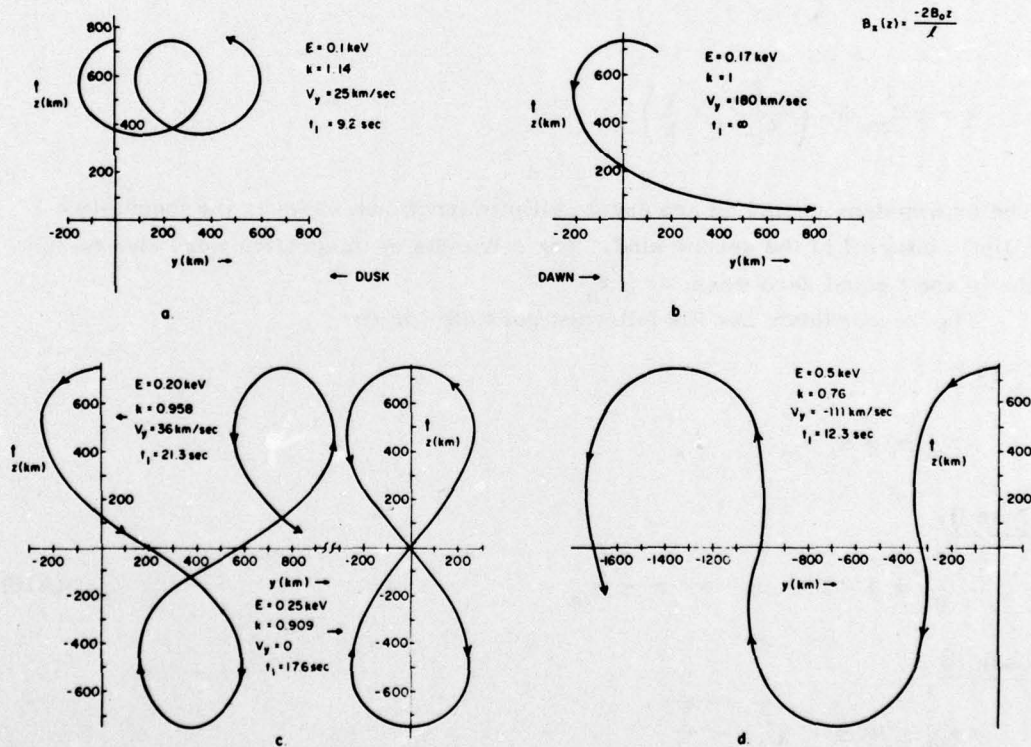


Figure A1. Various Proton Trajectories that Illustrate the Several Regimes of  $V_y$  as Shown in Figure A2. (a) Simple grad B drift at low energies; (b) Rapid loss at selected proton energies that cause an opposing current along  $+y$ ; (c) Zero drift velocity; (d) Higher energy protons that add to the current causing a pinch effect.



The critical energy above which protons execute harmonic motion about  $z = 0$  is found by setting (A6) to 1.0. For protons starting at  $z_m = \pm l/2$  this condition is simply

$$v = l/8 \frac{eB_0}{mc} \equiv \frac{l}{8} \omega_c \quad (A11)$$

If  $B_0 \simeq 10\gamma$  then  $\omega_c \simeq 1$  rad/sec and the critical energy is

$$E_{cp} = 1/2 mv^2 = 8.15 \times 10^{-15} l^2 \text{ ev} \quad (l \text{ in cm}) \quad (A12)$$

The critical energy is a sensitive function of the plasma sheet thickness,  $l$ . Take the thermal energy in the plasma sheet to be a couple of keV then for large  $l$  ( $l \sim 2.3 R_E$ )  $E_{cp} = 17.5$  keV which says that few, if any, protons cross the neutral sheet. Now compress the plasma sheet to  $l \sim 1500$  km. The critical energy is now 0.18 keV which implies a majority of protons execute harmonic motion across the neutral sheet. This is clearly a single-particle counterpart to the substorm triggering mechanism discussed in the text.

Further information can be obtained by defining the proton drift velocity in the  $y$ -direction as

$$v_y = \lim_{t \rightarrow \infty} y/t \quad (A13)$$

For the three cases discussed

Case I:

$$v_y = \left( 1 - \frac{2E(k)}{K(k)} \right) v \quad (A14)$$

Case II:

$$v_y = +v$$

Case III:

$$v_y = \left[ 2k^2 - 1 - \frac{2k^2 E\left(\frac{1}{k}\right)}{K\left(\frac{1}{k}\right)} \right] v$$



Here  $E(k)$  and  $E(1/k)$  are complete elliptic integrals of the second kind.  $K$  is the complete elliptic integral of the first kind. Note that at  $k = 0.909$  the drift energy,  $E'$ , is zero. The drift velocity is plotted in Figure A2 for protons passing close to the plasma sheet-tail lobe interface. ( $z_m = l/2$ ). The plasma sheet thickness,  $l$ , has been set equal to 1500 km. The drift velocity profile for other plasma sheet thicknesses can be found directly from Figure A2 by recalling that the critical energy scales as  $l$ -squared. See Eq. (A12).

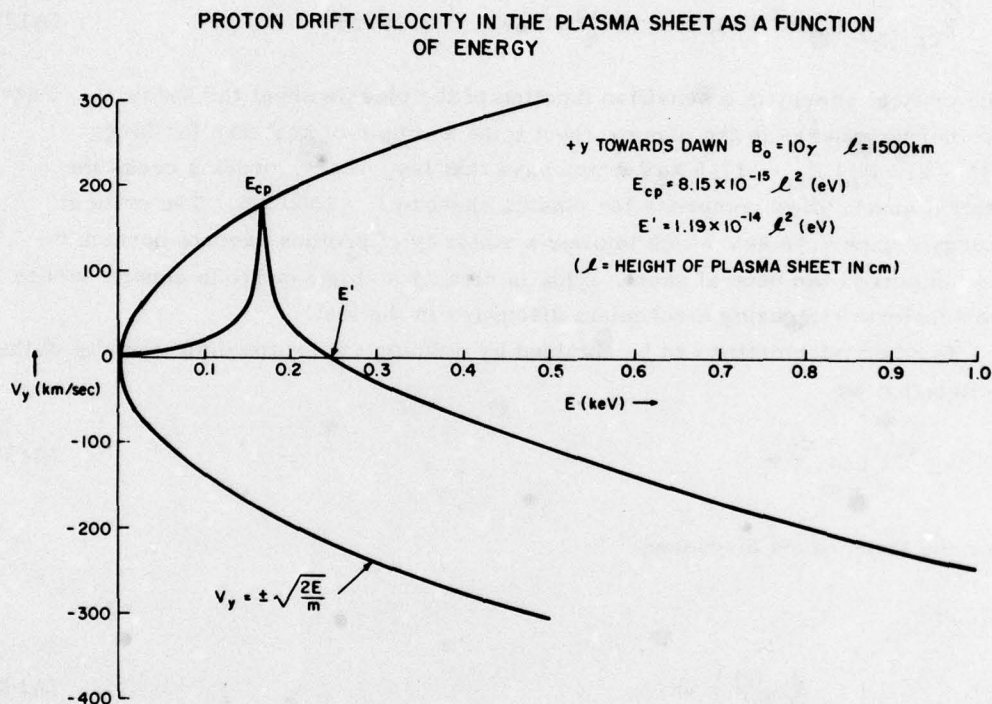


Figure A2. Proton Drift Velocity in the Plasma Sheet as a Function of Energy. This curve scales as the square of the plasma sheet thickness. Protons that pass through  $z_m = 750$  km (see Figure A1) have been specifically considered

Let us draw a physical scenario of a substorm onset based on the above remarks. The plasma sheet is again assumed to have a temperature of a couple keV. During quiet time conditions ( $l \sim 2.3 R_E$ )  $E'$  is  $\sim 25$  keV and from Figure A2 and Figure A1a most if not all, the protons are drifting toward dawn (+y) without crossing the neutral sheet. Now as the plasma sheet is compressed  $E'$  becomes comparable to the thermal proton energy and some of these protons now gyrate

across  $z = 0$  and drift towards dusk ( $-y$ ) (see Figure A1d). The protons that reverse their drift direction add to  $j_y$  and, therefore, by the Biot-Savat law cause  $l$  to continue decreasing. A decrease in  $l$  lowers  $E'$  even further leading to an equilibrium condition in which a further lowering of  $E'$  causes a negligible change in  $j_y$ . The conclusion is that the plasma sheet is unstable to this pinch effect once  $E'$  becomes some multiple of the thermal energy. For illustration purposes we set  $E' = 6$  keV and solve for  $l$  in Eq. (A6). The corresponding thickness is found to be  $\sim 1.1 R_E$ .

Figure A2 leads to one other final comment. The positive spike in the drift velocity corresponds to protons that having started at  $z_m = \pm l/2$  asymptotically approach but do not cross the positive  $y$  axis (Case II and Figure A1b). Therefore, particles very close to  $E_{cp}$  ( $k^2 = 1$ ) will cause a positive current fluctuation. This effect is identified as the source of the magnetic fluctuations described in Section 3.

## Appendix B

### Solution of the Eigenmodes

The model is defined in Figure 3. The potential energy of the entire system can be written as (Goldstein<sup>1</sup>)

$$V = \frac{K_A}{2} (z_2 - z_1 - r_0)^2 + \frac{K}{2} (z_3 - z_2 - l)^2 + \frac{K_A}{2} (z_4 - z_3 - r_0)^2 . \quad (B1)$$

Using the usual definition

$$\eta_i = z_i - z_{i0} \quad (B2)$$

$$i = 1, 4$$

where the zero subscript denotes equilibrium values. Expression (B1) then simplifies to

$$V = 1/2 K_A (\eta_2 - \eta_1)^2 + 1/2 K (\eta_3 - \eta_2)^2 + 1/2 K_A (\eta_4 - \eta_3)^2 . \quad (B3)$$

---

1. Goldstein, H. (1957) Classical Mechanics, Addison-Wesley Publ. Co., Inc., Reading, MA.



The familiar matrix form of  $|V - \omega^2 T|$  is shown in Figure B1. The kinetic energy tensor is treated as containing a unit mass density since  $\rho$  has been absorbed into  $V_A^2$ . Solving for the eigenvalues of  $\omega^2$ , we find that

$$(K_A + K - \omega^2)(K_A - \omega^2) - K_A^2 = \pm K(K_A - \omega^2) \quad (B4)$$

The positive root of this equation leads to

$$\omega^2 (\omega^2 - 2K_A) = 0 \quad (B5)$$

which has the obvious solutions

$$\omega^2 = 0$$

$$\omega^2 = 2K_A \quad (B6)$$

The minus root of (4B) leads to

$$\omega^4 = 2\omega^2(K + K_A) + 2KK_A = 0 \quad (B7)$$

with the solutions

$$\omega^2 = (K + K_A) \pm (K^2 + K_A^2)^{1/2} \quad (B8)$$

We now determine the eigenvectors for these four solutions of  $\omega^2$ . The  $\omega^2 = 0$  solution corresponds to a uniform translation of the entire system and is of little interest. Denoting  $A_{ij}$  as the displacement of the  $i$ th node for the  $j$ th eigenmode, we have for  $\omega^2 = 0$ ,

$$A_{11} = A_{21} = A_{31} = A_{41} \quad (B9)$$

For the second root ( $\omega_2^2 = 2K_A$ ) one finds

$$A_{12} = -A_{22} = -A_{32} = A_{42} \quad (B10)$$

The third root,  $\omega_3^2 = K + K_A + (K^2 + K_A^2)^{1/2}$ , leads to

$$A_{23} = -\frac{-(K + (K^2 + K_A^2)^{1/2})}{K_A} A_{13} = -A_{33} \quad (B11)$$

$$A_{43} = -A_{13}$$

Finally, for the fourth root  $\omega_4^2 = K + K_A - (K^2 + K_A^2)^{1/2}$  one has

$$A_{24} = \left( \frac{-K + (K^2 + K_A^2)^{1/2}}{K_A} \right) A_{14} = -A_{34} \quad (B12)$$

$$A_{44} = -A_{14}$$

Each of the eigenvectors are of unit magnitude (Goldstein<sup>1</sup>), that is

$$\sum_{i=1}^4 A_{ij}^2 = 1 \quad (B13)$$

This implies,

$$A_{11} = 1/2 \quad (B14)$$

$$A_{12} = 1/2 \quad (B15)$$

$$A_{13} = \frac{K_A}{2 \left[ K_A^2 + K^2 - K \sqrt{K^2 + K_A^2} \right]^{1/2}} \quad (B16)$$

$$A_{14} = \frac{K_A}{2 \left[ K_A^2 + K^2 - K \sqrt{K^2 + K_A^2} \right]^{1/2}} \quad (B17)$$

The four eigenmodes are schematically shown in Figure 4.

## MATRIX FOR THE EIGENMODES

$$|V - \omega^2 T| = \begin{vmatrix} K_A - \omega^2 & -K_A & 0 & 0 \\ -K_A & K_A + K - \omega^2 & -K & 0 \\ 0 & -K & K_A + K - \omega^2 & -K_A \\ 0 & 0 & -K_A & K_A - \omega^2 \end{vmatrix}$$

Figure B1. Energy Matrix for the Configuration Shown in Figure 3.